

# Can You See Me Now? Sensor Positioning for Automated and Persistent Surveillance

Yi Yao, Chung-Hao Chen, Besma Abidi, *Senior Member, IEEE*, David Page, Andreas Koschan, *Member, IEEE*, and Mongi Abidi, *Member, IEEE*

**Abstract**—Most existing camera placement algorithms focus on coverage and/or visibility analysis, which ensures that the object of interest is visible in the camera's field of view (FOV). However, visibility, which is a fundamental requirement of object tracking, is insufficient for automated persistent surveillance. In such applications, a continuous consistently labeled trajectory of the same object should be maintained across different camera views. Therefore, a sufficient uniform overlap between the cameras' FOVs should be secured so that camera handoff can successfully and automatically be executed before the object of interest becomes untraceable or unidentifiable. In this paper, we propose sensor-planning methods that improve existing algorithms by adding handoff rate analysis. Observation measures are designed for various types of cameras so that the proposed sensor-planning algorithm is general and applicable to scenarios with different types of cameras. The proposed sensor-planning algorithm preserves necessary uniform overlapped FOVs between adjacent cameras for an optimal balance between coverage and handoff success rate. In addition, special considerations such as resolution and frontal-view requirements are addressed using two approaches: 1) direct constraint and 2) adaptive weights. The resulting camera placement is compared with a reference algorithm published by Erdem and Sclaroff. Significantly improved handoff success rates and frontal-view percentages are illustrated via experiments using indoor and outdoor floor plans of various scales.

**Index Terms**—Camera handoff, camera placement, coverage analysis, multi-camera surveillance, sensor placement.

## I. INTRODUCTION

WITH the increased scale and complexity involved in most practical surveillance applications, it is almost impossible for any single camera [either fisheye or pan-tilt-zoom (PTZ)] to fulfill persistent tracking and monitoring tasks with an acceptable degree of continuity and/or reasonable accuracy. Systems with multiple cameras find extensive use in

Manuscript received April 14, 2008; revised August 13, 2008 and November 4, 2008. First published July 21, 2009; current version published October 30, 2009. This work was supported in part by the University Research Program in Robotics under Grant DOE-DE-FG52-2004NA25589. This paper was recommended by Associate Editor W. Hu.

Y. Yao is with the Global Research Center, General Electric, Niskayuna, NY 12309 USA (e-mail: yi.yao@ge.com).

C.-H. Chen, B. Abidi, and A. Koschan are with the Department of Electrical and Computer Engineering, University of Tennessee, Knoxville, TN 37996-2100 USA (e-mail: cchen10@utk.edu; besma@utk.edu; akoschan@utk.edu).

D. Page is with the Third Dimension Technologies LLC, Knoxville, TN 37920-2805 USA (e-mail: davidpage@ieee.org).

M. Abidi is with the Imaging, Robotics, and Intelligent System Laboratory, Department of Electrical and Computer Engineering, University of Tennessee, Knoxville, TN 37996-2100 USA (e-mail: abidi@utk.edu).

Color versions of one or more of the figures in this paper are available online at <http://ieeexplore.ieee.org>.

Digital Object Identifier 10.1109/TSMCB.2009.2017507

surveillance applications. Hu *et al.* [21] surveyed the state of the art in visual surveillance with dynamic scenes to understand and characterize object motion and behaviors. A more recent survey of multimodel sensor planning and integration for wide-area surveillance can be found in [1].

The need for sensor planning naturally comes when the question of how multiple cameras can be placed and coordinated to fulfill given tasks with given performance requirements arises. One descriptive definition of sensor planning in [39] is quoted as follows: "Given information about the environment as well as the information about the task that the vision system is to accomplish, develop strategies to automatically determine sensor parameter values that achieve this task with a certain degree of satisfaction."

In the literature, most sensor placement algorithms, from the Art Gallery problem [31] and the large-scale terrain guarding [28] to the more recent research in surveillance applications [15], [30], focus on coverage and visibility analysis. Cameras are placed such that a full or specified coverage of the environment or object is achieved. The conventional requirements in sensor planning, i.e., coverage and visibility, cannot ensure by themselves a persistent automated tracking in real-time surveillance systems. Such applications and systems require a continuous consistently labeled trajectory of the same object across different camera views. To meet this requirement, sufficient amounts of overlap between the FOVs of adjacent cameras should be reserved so that consistent labeling and camera handoff can successfully be executed [45]. However, coverage and overlapped FOVs go in opposite directions. Given the same camera configuration, an increase in overlapped FOVs sometimes leads to a decrease in coverage. Therefore, an optimal balance between coverage and overlapped FOVs will be found via sensor planning. The optimal balance requires a maximum increase in handoff success rate but at the cost of a minimum decrease in coverage if the same number of cameras is used.

We refer to the necessary overlapped FOVs as a handoff safety margin and design an observation measure to differentiate it from other visible areas in the camera's FOV. Based on this safety margin, we develop sensor-planning algorithms that balance the tradeoff between the overall coverage and adequate overlap. Fig. 1 depicts a graphical illustration of the advantage of introducing a handoff safety margin to sensor planning. For clear presentation, we purposefully consider a simpler case, where the floor plan of the environment that will be surveilled is a rectangle, and the camera's FOV resembles a disc. We examine two scenarios: 1) undercoverage and 2) overcoverage. In the case of undercoverage, the number of cameras is not

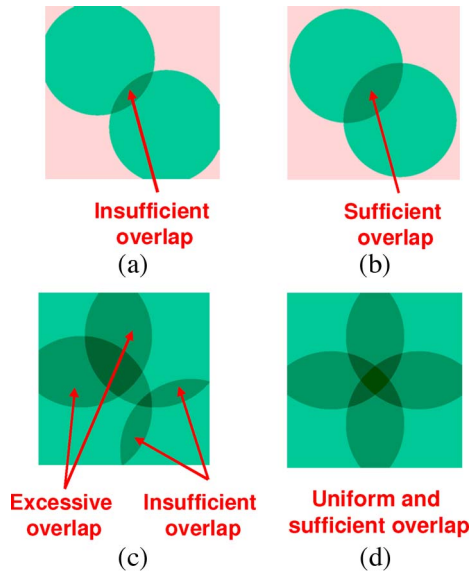


Fig. 1. Graphical comparison of the camera placement between coverage maximization and our method. Scenario of undercoverage: (a) method for coverage maximization (the coverage is 63.9%, whereas the overlapped FOV percentage is 6.8%) and (b) our method (the coverage is 60.8%, whereas the overlapped FOV percentage is 21.5%). Scenario of overcoverage: (c) method for coverage maximization and (d) our method.

sufficient to generate a full coverage of the environment. The conventional sensor-planning methods try to maximize the coverage, which leads to insufficient overlapped FOVs for carrying out successful camera handoffs, as shown in Fig. 1(a). Our method can improve the overlapped FOV percentage from 6.8% to 21.5% and, hence, the success rate of camera handoff but at the cost of slightly decreased coverage from 63.9% to 60.8%.

The advantage of our algorithm becomes more significant for the case of overcoverage. Fig. 1(c) illustrates one possible camera placement from coverage maximization. Due to the lack of constraints on the amount of overlapped areas between adjacent cameras, the overlapped FOVs are nonuniform. Handoff failures may still occur in areas with insufficient overlapped FOVs. In comparison, the camera placement from our algorithm can achieve uniform sufficient overlapped FOVs to ensure an approximately 100% handoff success rate while maintaining the same coverage.

In [45], we presented sensor-planning algorithms that achieve the optimal balance between coverage and overlapped FOVs for static-perspective cameras. Here, different types of cameras are discussed, e.g., omnidirectional and PTZ cameras. The main challenge constitutes in unifying the definition of observation measure so that various types of cameras can be incorporated into the same framework for camera placement. This paper tackles the aforementioned difficulty and extends the work from static-perspective cameras to different types of cameras. In addition to the proposed basic algorithm, variations, including direct constraint and adaptive weight approaches, are introduced for special considerations of resolution and frontal-view requirements. We compare the efficiency of our algorithm with the scheme proposed by Erdem and Sclaroff [15] under three criteria by using floor plans of various scales: 1) coverage; 2) handoff success rate; and 3) frontal-view percentage. At the cost of a slightly decreased coverage, a significantly im-

proved handoff success rate and a frontal-view percentage are accomplished.

The major contributions of this paper are listed as follows. First, an observation measure is designed for both perspective and omnidirectional cameras to describe the suitability of tracking and to define the handoff safety margin. Second, a generic sensor positioning algorithm for automated and persistent tracking is developed to secure sufficient handoff margins. Last, special considerations such as resolution and frontal view are addressed by two types of solutions: 1) the direct constraint and 2) the adaptive weights.

The remainder of this paper is organized as follows. A brief review of related work is given in Section II. Sections III and IV define the observation measure and handoff safety margin, respectively. Our objective functions for the search of the optimal camera placement are described in Section V. Section VI presents the proposed sensor-planning algorithm. Section VII demonstrates our experimental results and comparisons with the reference algorithm. Section VIII concludes this paper.

## II. RELATED WORK

In the literature, most placement algorithms for visual sensors are proposed for such applications as 3-D object inspection and reconstruction. Roy *et al.* reviewed existing sensor-planning algorithms for 3-D object reconstruction [36] and proposed an online scheme that uses a probabilistic reasoning framework for next-view planning and object recognition [37]. A more recent and thorough discussion regarding sensor-planning algorithms for 3-D object reconstruction and recognition can be found in [8]. The authors also pointed out promising directions for future research, such as the combinational optimization of the placement of both cameras and illumination sources. Wong *et al.* defined a metric that evaluates the unknown information in each group of potential viewpoints and used it in the search of the next best view for 3-D modeling [42]. Yous *et al.* designed an active scheme for multiple PTZ camera assignment so that each camera observes a specific part of a moving object, mainly pedestrians, and achieves the best visibility of the whole object [47]. The selection of sets of omnidirectional views for the representation of a 3-D scene is discussed in [40]. In [38], fuzzy logic inference is employed for camera placement, considering the uncertainty in the analysis of visibility, accessibility, and camera-object distance. Chen and Li [9] addressed the placement of active sensors in the context of robot vision. With the increased scale of multi-camera systems, sensor planning is also conducted in a larger scale and at a higher level similar to sensor networks. Guo *et al.* modeled observability as a decreasing exponential function of the observation distance and used this model in the camera placement for the monitoring and tracking of mass objects [17]. Dunn *et al.* employed the Parisian evolutionary algorithm to search for the optimal camera placement for 3-D object reconstruction that aims at a reduced computational complexity [14].

Sensor planning for surveillance systems has also received increasing attention in recent years [6], [7], [22], [25], [34]. There exist two major directions in sensor planning for surveillance systems: 1) offline camera positioning and 2) online

camera selection. Offline camera positioning answers the question of how multiple cameras can be placed in the environment to fulfill specified tasks. Erdem and Sclaroff defined different types of coverage problems and developed corresponding solutions using perspective cameras [15]. Their methods have been implemented in a simulator with genetic algorithm as the optimization engine [12]. Several placement algorithms are developed based on Erdem and Sclaroff's method. Angella *et al.* presented solutions for the more generalized  $\mathcal{M}$ -coverage problem, where it is desired that the object of interest can be observed by at least  $\mathcal{M}$  cameras [3]. Horster and Lienhart also addressed the  $\mathcal{M}$ -coverage problem and transformed their nonlinear objective function to a linear one so that linear binary programming can be used in the search of the optimal camera placement [20].

The literature also mentions sensor placement algorithms that focus on additional considerations such as path observability, dynamic occlusion, and frontal-view availability. Bodor *et al.* presented a camera placement algorithm for maximizing the observability of a path [5]. Similarly, Fiore *et al.* used the distance and foreshortening constraints to describe the observability of a path and defined the corresponding cost function [16]. Successful camera placement and online repositioning are demonstrated for tracking pedestrians that move along a regular path using two fixed cameras that were mounted on remotely controllable mobile platforms. A probabilistic camera planning framework with dynamic visibility analysis was proposed by Mittal and Davis [30]. Another metric that describes the likelihood of dynamic occlusion is also discussed in [10] for the optimization of camera configurations. Ram *et al.* introduced frontal-view probability to coverage analysis and demonstrated real-time camera selection for better observation of a pedestrian [35].

Online camera selection, which is also referred to as the focus of attention problem by Isler *et al.* [23], is introduced as a result of the improved mobility of cameras. The object of interest can be observed by multiple cameras; thus, an online resource management mechanism is necessary to guide the coordination among multiple cameras for an optimal system performance. The optimal performance is twofold: 1) the optimal observation of every object of interest and 2) the optimal computational load for every camera deployed in the environment. Gupta *et al.* discussed a unified approach, referred to as confusion and occlusion analysis for selections based on tasks (COST), that selects a set of cameras that will be used for the inferences for each person in a group of pedestrians, considering occlusions and visual confusion [18]. Isler *et al.* proposed a selection framework to assign cameras to track the object of interest for a minimized expected error in the estimation of the object's location [23]. In [13], an activity map is established on the fly and used to direct and coordinate multiple PTZ cameras.

In the aforementioned review, we concentrate on the placement of cameras, i.e., one type of visual sensors. In the following discussion, we look into sensor-planning algorithms in a broader scope, where different types of sensors, in addition to visual ones, are used. Yang *et al.* discussed a sensor placement method based on the Hungarian algorithm and scan operation [44]. To resolve the problematic assumption that sensors have a fixed sensing region, nonparametric probabilistic

models and Gaussian processes are established to optimize sensor placement in two aspects: 1) informative and 2) of low communication cost [26], [27]. The geometrical approach utilizes geometrical methods such as Voronoi diagram [2], [41], Delaunay triangulation [43], disc packing [48], [49], and tessellation [50], [51]. For instance, Wang *et al.* designed algorithms to iteratively adjust the positions of sensors for the optimal coverage [41]. Ma and Yang described an adaptive deployment algorithm for unattended mobile sensors [29].

In this paper, we concentrate on offline camera positioning. When mathematically formulated as an optimization problem, two types of approaches in camera positioning [15], [28] exist: 1) the search for the maximum coverage, given a fixed total cost or the number of cameras, and 2) the search for the minimum cost or the number of cameras for a full or required coverage. In this paper, we refer to Approaches 1 and 2 as the Max-Coverage and Min-Cost problems.

Assuming that a polygonal floor plan is represented as an occupancy grid, a binary vector  $\mathbf{b}$  can be obtained by letting  $b_i = 1$  if the  $i$ th grid is covered by at least one camera; otherwise, it is  $b_i = 0$ . We construct a binary coefficient matrix  $A$  with  $a_{ij} = 1$  if the  $i$ th grid is covered by the  $j$ th camera configuration. Each camera configuration specifies one combination of the camera's intrinsic and extrinsic parameters, including the focal length  $f$ , pan/tilt angle  $\theta_P/\theta_T$ , and position  $T_C$ . The following relation holds:  $b_i = 1$  if  $b'_i > 0$  and  $b_i = 0$  otherwise, with  $\mathbf{b}' = A\mathbf{x}$ . The solution vector  $\mathbf{x}$  specifies a set of chosen camera configurations with the corresponding element, i.e.,  $x_j = 1$ , if the configuration is chosen; otherwise, it is  $x_j = 0$ . Let the cost associated with the  $j$ th camera configuration be  $\omega_j$ . Given the maximum cost  $\Omega_{\max}$ , the Max-Coverage problem can be described by

$$\max \sum_i b_i, \quad \text{subject to} \quad \sum_j \omega_j x_j \leq \Omega_{\max}. \quad (1)$$

Given a required coverage vector  $\mathbf{b}_{C,o}$  or a minimum overall coverage  $C_{\min}$ , the Min-Cost problem can be modeled as

$$\min \sum_j \omega_j x_j, \quad \text{subject to} \quad A\mathbf{x} \geq \mathbf{b}_{C,o} \text{ or } \sum_i b_i \geq C_{\min}. \quad (2)$$

### III. OBSERVATION MEASURE

In addition to visibility, we introduce the following criteria to describe the observation of the tracked target: 1) its resolution  $M_R$  and 2) its distance to the edges of the camera's FOV  $M_D$ . From a viewer's perspective, visibility is a fundamental requirement. Herewith, the viewer includes not only human operators but also automatic processes such as consistent labeling, object tracking, and face/object recognition. Observations with different detail levels affect the performance of these algorithms. For example, a frontal face image with an interocular distance that is not smaller than 60 pixels is recommended by a well-known face recognition engine FaceIt so that a face will automatically be recognized [33]. For persistent object tracking and smooth camera handoff, the tracked target should be at a reasonable distance from the edges of the camera's FOV. The  $M_D$  component considers the margin for executing handoff before the object falls out of the camera's FOV.

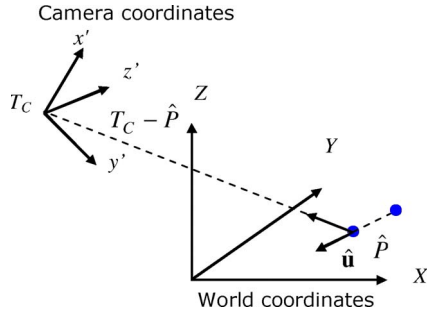


Fig. 2. Illustration of the camera and world coordinates for perspective cameras.

### A. Static-Perspective Cameras

To begin with, the camera and world coordinates are defined and illustrated in Fig. 2. A point  $P = [X \ Y \ Z]^T$  in the world coordinates is projected onto a point  $[x' \ y' \ z']^T$  in the camera coordinates by

$$\begin{bmatrix} x' \\ y' \\ z' \end{bmatrix} = \begin{bmatrix} \cos \theta_T & 0 & -\sin \theta_T \\ 0 & 1 & 0 \\ \sin \theta_T & 0 & \cos \theta_T \end{bmatrix} \begin{bmatrix} 1 & 0 & 0 \\ 0 & \cos \theta_P & \sin \theta_P \\ 0 & -\sin \theta_P & \cos \theta_P \end{bmatrix} \times \begin{bmatrix} Z - T_Z \\ X - T_X \\ Y - T_Y \end{bmatrix} \quad (3)$$

with  $T_C = [T_X \ T_Y \ T_Z]^T$ . Assuming zero skew, unit aspect ratio, and image center on the principal point, the projected point on the image plane is given by  $\begin{cases} x = f x' / z' \\ y = f y' / z' \end{cases}$ . Letting  $Z = 0$  (points on the ground plane), we have

$$\begin{cases} x = f \frac{-T_Z \cos \theta_T - Z' \sin \theta_T}{-T_Z \sin \theta_T + Z' \cos \theta_T} \\ y = f \frac{Y'}{-T_Z \sin \theta_T + Z' \cos \theta_T} \end{cases} \quad (4)$$

where

$$\begin{bmatrix} Y' \\ Z' \end{bmatrix} = \begin{bmatrix} \cos \theta_P & \sin \theta_P \\ -\sin \theta_P & \cos \theta_P \end{bmatrix} \begin{bmatrix} X - T_X \\ Y - T_Y \end{bmatrix}. \quad (5)$$

The estimation of the target depth  $\hat{z}'$  can be obtained by

$$\hat{z}' = -T_Z \sin \theta_T + Z' \cos \theta_T = \frac{-T_Z}{x/f \cos \theta_T + \sin \theta_T}. \quad (6)$$

For static cameras with a constant focal length, the estimated target depth is sufficient to describe the resolution, i.e.,

$$M_R = \alpha_R / \hat{z}' \quad (7)$$

where  $\alpha_R$  is a normalization coefficient. However, when the target is at a close distance, this relation is not entirely valid, in particular when part of the target falls out of the camera's FOV. Therefore, the aforementioned definition is modified as

$$M_R = \begin{cases} \alpha_R / \hat{z}' & \hat{z}' > |T_Z / \tan \theta_T| \\ \frac{\alpha_R}{(\hat{z}' + T_Z / \tan \theta_T)^2 - T_Z / \tan \theta_T} & \hat{z}' \leq |T_Z / \tan \theta_T|. \end{cases} \quad (8)$$

In practice, for a better observation and to reserve enough computation time for camera handoff, the target should remain

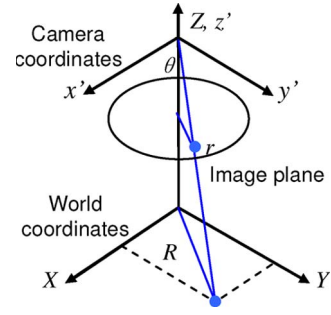


Fig. 3. Illustration of the geometry for omnidirectional cameras.

at a safe distance from the edges of the camera's FOV. Moreover, this margin distance is affected by the target depth. When the target is at a closer distance, its projected image undergoes larger displacements in the image plane. Therefore, a larger margin should be reserved. In our definition, different polynomial powers are used to achieve varying decreasing/increasing rates of  $M_D$  as the object of interest moves from the image center in the direction orthogonal to the optical axis of the camera. The  $M_D$  is then given by

$$M_D = \left\{ \alpha_D \left[ (1 - 2|x|/N_{row})^2 + (1 - 2|y|/N_{col})^2 \right] \right\}^{\beta_1 \hat{z}' + \beta_0} \quad (9)$$

where  $N_{col}$  and  $N_{row}$  denote the image's width and height,  $\alpha_D$  is a normalization weight, and coefficients  $\beta_1$  and  $\beta_0$  are used to adjust the polynomial power.

The observation measure for a static-perspective camera is then given by

$$Q = \begin{cases} w_R M_R + w_D M_D & [x \ y]^T \in \Pi \\ -\infty & \text{otherwise} \end{cases} \quad (10)$$

where  $w_R$  and  $w_D$  are importance weights, and  $\Pi$  denotes the image plane.

### B. PTZ Cameras

For PTZ cameras with varying zooms, the resolution component  $M_R$  is given by

$$M_R = \alpha_R f / \hat{z}'. \quad (11)$$

Compared to (8), the additional term for the special case when part of the target falls out of the camera's FOV is not necessary because of the additional flexibility from the camera's adjustable pan and tilt angles. We assume that the target is always maintained at the image center by panning and tilting the camera. Therefore, the  $M_D$  component can be eliminated from the computation of the observation measure.

### C. Omnidirectional Cameras

The geometry of an omnidirectional camera is depicted in Fig. 3. The imaging process of an omnidirectional camera does not comply with the traditional perspective projection. Two types of omnidirectional cameras exist: 1) dioptic (fisheye-lens) and 2) catadioptric (reflected-mirror) cameras. We first give the definition of the resolution and distance components for dioptic cameras. Let  $r$  denote the distance between the projected point  $[x \ y]^T$  and the principal point. Let  $\theta$  denote

the angle between the incoming ray and the optical axis. The perspective projection is characterized by  $r = f \tan \theta$ . To realize a wider opening angle, this relation is changed in omnidirectional cameras. Various projection models exist in the literature [24], e.g., the equidistance projection, i.e.,  $r = f\theta$ , and the general polynomial model, i.e.,  $r = f \sum_{k=1, \text{odd}} \lambda_{\theta, k} \theta^k$ , where  $\lambda_{\theta, k}$  denote the approximation coefficients. Image resolution can be computed as the partial derivative of  $r$  with respect to  $R$ . We have

$$M_R = \alpha_R \frac{\partial r}{\partial R} = \frac{\alpha_R f Z}{Z^2 + R^2} \sum_{k=1, \text{odd}} \lambda_{\theta, k} k \theta^{k-1} \quad (12)$$

with  $R = \sqrt{X^2 + Y^2}$ . The  $M_D$  component is given by

$$M_D = \alpha_D (1 - r/r_o)^2 \quad (13)$$

where  $r_o$  represents the image radius of the omnidirectional camera. The observation measure is a weighted sum of the  $M_R$  and  $M_D$  components.

A catadioptric camera consists of a regular lens and a reflected mirror. The shape of the reflected mirror determines the resulting projection model. It is shown that a unified framework can be used to describe both types of cameras [46]. The general polynomial model is a good candidate. The only difference lies in the fact that, unlike dioptric cameras, catadioptric cameras suffer from a disc-like blind region at the center of the image. The blind region results from the occluded FOV caused by the special-shaped mirror in front of the camera's lens. The radius of the blind region in the image plane  $r_b$  can be computed from the characteristics of the mirror, camera's lens, and their relative position. The definition of the resolution and distance components for catadioptric cameras are given by

$$M_R = \begin{cases} \frac{\alpha_R f Z}{Z^2 + R^2} \sum_{k=1, \text{odd}} \lambda_{\theta, k} k \theta^{k-1} & r_b < r \\ -\infty & 0 \leq r \leq r_b \end{cases} \quad (14)$$

$$M_D = \begin{cases} \alpha_D \left(1 - \frac{r - 1.5r_b}{r_o}\right)^2 & 1.5r_b < r \\ \alpha_D \left(1 - \frac{1.5r_b - r}{r_o}\right)^2 & 0 \leq r \leq 1.5r_b \end{cases} \quad (15)$$

respectively.

#### IV. HANDOFF SAFETY MARGIN

In addition to the conventional requirements in sensor planning, e.g., coverage and cost, extra criteria need to be considered to ensure persistent tracking and monitoring in a real-time automatic surveillance system. One of the criteria that will be included is a sufficient uniform amount of overlapped FOVs between adjacent cameras so that enough time is reserved to perform consistent target labeling and successful camera handoff. This criterion, to which this paper is devoted, is, however, not addressed in existing camera placement algorithms. In coverage analysis, two types of areas—visible and invisible—are used. To incorporate handoff rate analysis, a third type of area, i.e., handoff safety margin, is introduced, which defines the visible areas that require camera handoff to be triggered.

A failure threshold  $Q_F$  and a trigger threshold  $Q_T$  are derived to define three disjoint regions: 1) an invisible area with  $Q_{ij} < Q_F$ , where  $Q_{ij}$  represents the observation measure value of the  $i$ th grid that was observed by the  $j$ th camera

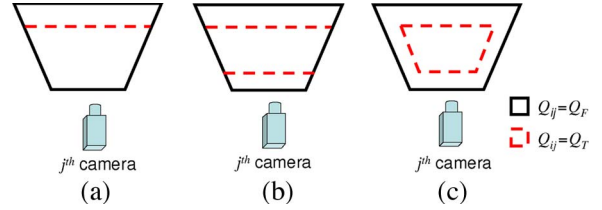


Fig. 4. Schematic of the contours of the observation measure with  $Q_{ij} = Q_F$  and  $Q_{ij} = Q_T$  to show the effect of the  $M_R$  and  $M_D$  components. (a)  $Q = M_R = \alpha_R / \hat{z}'$ . (b)  $Q = M_R$ , as defined in (8). (c)  $Q = w_R M_R + w_D M_D$ , with  $w_R = 0.5$  and  $w_D = 0.5$ .

configuration; 2) a visible area with  $Q_{ij} \geq Q_T$ ; and 3) a handoff safety margin with  $Q_F \leq Q_{ij} < Q_T$ . The failure threshold  $Q_F$  segments the invisible areas and is used for coverage analysis. The trigger threshold  $Q_T$  separates the visible areas and handoff safety margins. It is introduced for handoff rate analysis, where necessary overlapped FOVs between adjacent cameras are optimized. The trigger threshold  $Q_T$  is given by  $Q_T = Q_F + \kappa u_{obj} t_H$ , where  $u_{obj}$  represents the average moving speed of the object of interest,  $t_H$  denotes the average duration for a successful handoff, and  $\kappa$  is a conversion scalar.

The individual and combined effects of the  $M_R$  and  $M_D$  components become evident when we study the contours of the observation measure defined by  $Q_F$  and  $Q_T$ . In Fig. 4, the black solid lines and red dashed lines depict the contours, with  $Q_{ij} = Q_F$  and  $Q_{ij} = Q_T$ , respectively. The resolution component  $M_R$  provides limits along the direction of the optical axis of the camera, whereas the  $M_D$  component generates constraints mainly in the direction orthogonal to the optical axis of the camera. If (7) is used, as shown in Fig. 4(a), the handoff safety margin is given by  $\alpha_R / \hat{z}' < Q_T$ . That is,  $\alpha_R / Q_T < \hat{z}'$ . As a result, the handoff safety margin is only defined at the far end of the camera's FOV along the optical axis. The scenario where the target is very close to the camera such that part of it falls out of the camera's FOV is ignored. The modification in (8) imposes a proper constraint at the near end of the camera's FOV along the optical axis, as shown in Fig. 4(b). Therefore, the resulting observation is complete and with the desired resolution.

#### V. OBJECTIVE FUNCTION

To incorporate the ability of occlusion handling, we employ the occlusion analysis method in [15] to predict possible occlusions in the ground plane caused by obstacles. Denote the occluded region in the ground plane that was observed by the  $j$ th camera caused by the  $k$ th obstacle as  $O_{j,k}$ . The union of all the occluded regions that were observed by the  $j$ th camera is given by  $O_j = \bigcup_k O_{j,k}$ . Let  $A_O$  represent the occlusion coefficient matrix, with  $a_{O,ij} = 1$  if  $[X_i \ Y_i]^T \in O_j$ ; otherwise, it is  $a_{O,ij} = 0$ .

Let  $A_C$  represent the grid coverage, with  $a_{C,ij} = 1$  if  $Q_{ij} \geq Q_F$  and  $a_{O,ij} = 0$ . Otherwise,  $a_{C,ij} = 0$ . Matrix  $A_C$  resembles matrix  $A$  in the conventional coverage analysis discussed in the previous section. Two additional coefficient matrices are constructed: 1)  $A_H$  and 2)  $A_V$ . The matrix  $A_H$  has  $a_{H,ij} = 1$  if  $Q_F \leq Q_{ij} < Q_T$  and  $a_{O,ij} = 0$ . Otherwise,  $a_{H,ij} = 0$ . The matrix  $A_V$  has  $a_{V,ij} = 1$  if  $Q_{ij} \geq Q_T$  and  $a_{O,ij} = 0$ . Otherwise,  $a_{V,ij} = 0$ . Matrices  $A_H$  and  $A_V$  represent the handoff safety margin and visible area, respectively. Recall that the solution vector  $\mathbf{x}$  specifies a set of chosen camera configurations

with the corresponding element  $x_j = 1$  if the configuration is chosen; otherwise, it is  $x_j = 0$ . Let  $\mathbf{c}'_C = A_C \mathbf{x}$ ,  $\mathbf{c}'_H = A_H \mathbf{x}$ , and  $\mathbf{c}'_V = A_V \mathbf{x}$ . The objective function is formulated as

$$c_i = w_C (c'_{C,i} > 0) + w_H (c'_{H,i} = 2) - w_V (c'_{V,i} > 1) \quad (16)$$

where  $w_C$ ,  $w_H$ , and  $w_V$  are predefined importance weights. The operation  $(c'_{C,i} > 0)$  means that

$$(c'_{C,i} > 0) = \begin{cases} 1, & c'_{C,i} > 0 \\ 0, & \text{otherwise.} \end{cases}$$

The first term in the objective function considers coverage, the second term produces sufficient overlapped handoff safety margins, and the third term penalizes excessive overlapped visible areas. Our objective function achieves a balance between coverage and sufficient margins for camera handoff. The optimal sensor placement for the Max-Coverage and Min-Cost problems can then be obtained by

$$\max \sum_i c_i, \quad \text{subject to } \sum_j \omega_j x_j \leq \Omega_{\max} \quad (17)$$

$$\min \sum_j \omega_j x_j \quad \text{then } \max \sum_i c_i, \\ \text{subject to } A_C \mathbf{x} \geq \mathbf{b}_{C,o} \text{ or } \sum_i b_i \geq C_{\min}. \quad (18)$$

Solving the Min-Cost problem is a sequential optimization process. First, the number of cameras and their types are optimized to achieve a minimized cost and maintain the required coverage. The objective function  $\sum_j \omega_j x_j$  is linear with respect to the solution vector  $\mathbf{x}$ ; thus, linear programming can be used in this step. Second, the camera parameters are optimized by maximizing the second objective function  $\sum_i c_i$ . Note that the second step employs the same objective function as that of the Max-Coverage problem but with different constraints.  $c_i$  is a nonlinear function of the solution vector  $\mathbf{x}$ ; thus, a more evolved optimization method than linear programming is required. The selection of the appropriate optimization methods for solving the Max-Coverage problem and the second step of the Min-Cost problem will be discussed in detail in Section VI.

Special performance requirements are frequently encountered in surveillance applications. To meet these requirements, additional constraints need to be added. The coverage and resolution considerations correspond to priority areas that need complete coverage and/or specified resolution. The frontal-view requirement results from path constraints where there exist predefined paths within which the objects' movements are restricted.

Two approaches for imposing these requirements exist: 1) direct constraints and 2) adaptive weights. Considering the coverage requirement for example, the direct constraint approach finds the solution by imposing an extra constraint  $A_C \mathbf{x} \geq \mathbf{b}_{C,o}$ , where  $\mathbf{b}_{C,o}$  represents the required coverage, with  $b_{C,o,i} = 1$ , if the corresponding grid will be covered; otherwise, it is  $b_{C,o,i} = 0$ . The adaptive weight approach assigns different weights  $w_{C,i}$  to the grid points according to the coverage requirements. Larger weights are used if the corresponding grids need to be covered. The objective function of (16) then becomes

$$c_i = w_{C,i} (c'_{C,i} > 0) + w_H (c'_{H,i} = 2) - w_V (c'_{V,i} > 1). \quad (19)$$

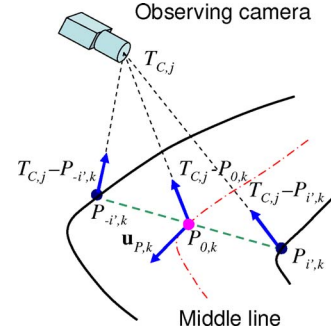


Fig. 5. Illustration of how the frontal view component can be computed with path constraints.

To incorporate the resolution requirements, we construct a matrix  $A_R$  with  $a_{R,ij} = 1$  if  $M_{R,ij} \geq M_{R,o,i}$ ; otherwise, it is  $a_{R,ij} = 0$ . Here,  $M_{R,o,i}$  is the corresponding resolution requirement at the  $i$ th grid point. The direct constraint approach is carried out by introducing an extra constraint  $A_R \mathbf{x} \geq \mathbf{b}_{R,o}$ , where  $\mathbf{b}_{R,o}$  represents the required resolution, with  $b_{R,o,i} = 1$  if the corresponding grid needs the minimum resolution; otherwise, it is  $b_{R,o,i} = 0$ . In the adaptive weight approach, the objective function becomes

$$c_i = w_C (c'_{C,i} > 0) + w_H (c'_{H,i} = 2) - w_V (c'_{V,i} > 1) + w_{R,i} (c'_{R,i} > 0) \quad (20)$$

where  $\mathbf{c}'_R = A_R \mathbf{x}$  and  $w_{R,i}$  are different weights that were allocated according to the resolution requirement.

In surveillance systems, a predefined path is commonly encountered. It is also preferred that a frontal view can be achieved some time while pedestrians are moving along this path. One example is entrance areas where a frontal view of the pedestrian is desired when he/she enters the gate. We use the tangential direction of the middle line of the path as the average direction of the pedestrian's motion, as shown in Fig. 5. Let the  $k$ th point on the middle line be  $P_{0,k}$  and its tangential direction be  $\mathbf{u}_{P,k}$ . The frontal-view measure that was observed by the  $j$ th camera at point  $P_{i',k}$  along the line perpendicular to  $\mathbf{u}_{P,k}$  is given by

$$FV_{i'j} = \frac{(T_{C,j} - P_{i',k})^T \mathbf{u}_{P,k}}{\|T_{C,j} - P_{i',k}\| \|\mathbf{u}_{P,k}\|}. \quad (21)$$

Based on  $FV_{i'j}$ , we define a matrix  $A_{FV}$ , with  $a_{FV,i'j} = 1$  if  $FV_{i'j} \geq 0$ ; otherwise, it is  $a_{FV,i'j} = 0$ . Let  $a_{FV,i'j} = 0$  for grid points outside the path. Finally, the path constraint is incorporated into sensor planning by

$$c_i = w_C (c'_{C,i} > 0) + w_H (c'_{H,i} = 2) - w_V (c'_{V,i} > 1) + w_{FV,i} (c'_{FV,i} > 0) \quad (22)$$

where  $\mathbf{c}'_{FV} = A_{FV} \mathbf{x}$  and  $w_{FV,i}$  are different weights that were allocated according to the frontal-view requirement.

Note that, although the coverage, resolution, and path constraints are separately addressed, it is straightforward to combine any two terms or all three. The only modification is to add the corresponding terms. The adaptive weight approach is particularly attractive because of its concise expression and speed of convergence.

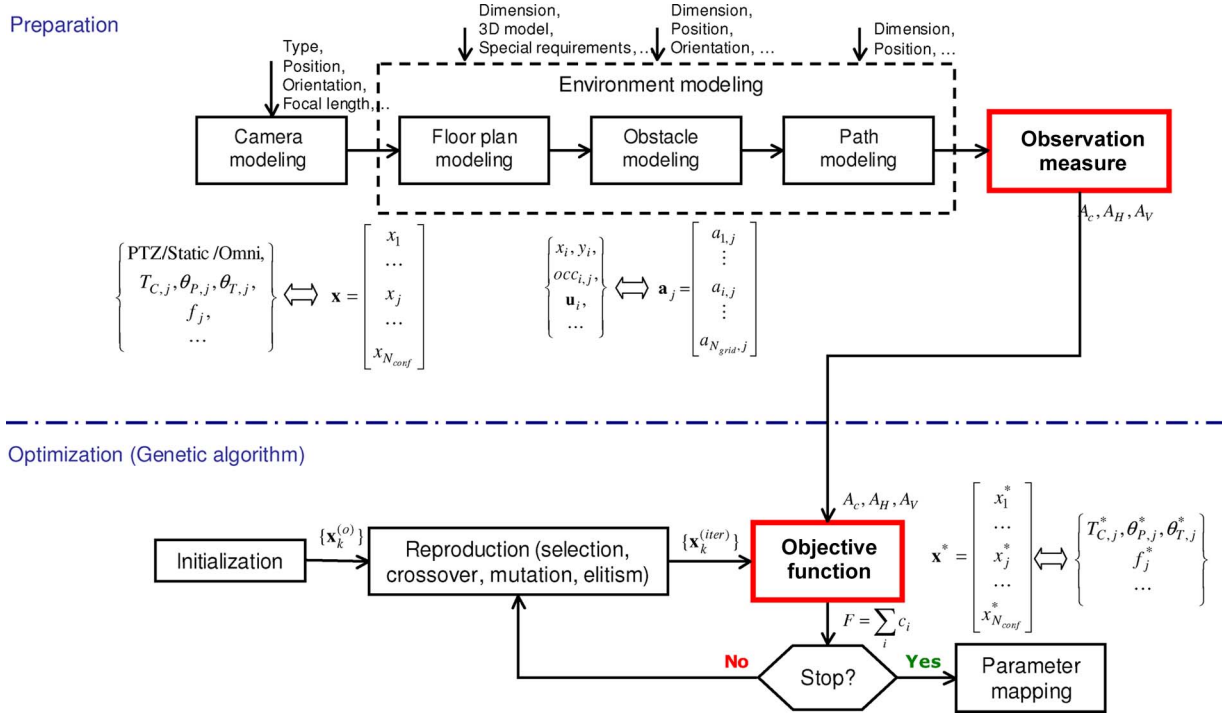


Fig. 6. Block diagram of the proposed sensor-planning algorithm.

## VI. SENSOR PLANNING

Fig. 6 shows the flow chart of the proposed sensor-planning algorithm, with the highlighted boxes indicating our contributions. Our algorithm can be divided into two stages: 1) preparation and 2) optimization. The preparation stage includes three blocks in serial: 1) camera modeling; 2) environment modeling; and 3) observation measure computation. The input of the camera-modeling block indicates the possible choices of the cameras' types and the extrinsic and intrinsic parameters. The cameras' extrinsic and intrinsic parameters are sampled within their feasible ranges to form different combinations. We refer to each combination as one camera configuration. Afterward, the solution vector  $\mathbf{x}$  is formulated with its  $j$ th element that corresponds to the  $j$ th camera configuration. The camera-modeling block performs as a sampler and an encoder. It emulates possible camera configurations and produces a mapping between the solution vector and camera configurations. This mapping is used in the last step of optimization when the optimal solution  $\mathbf{x}^*$  has been found to decode the solution vector into the actual optimal camera configuration.

The environment-modeling block includes three subblocks: 1) floor plan modeling; 2) obstacle modeling; and 3) path modeling. As the names suggest, the floor plan modeling deals with the overall 3-D model of the environment, whereas the obstacle- and path-modeling blocks handle obstacles and paths, respectively. The environment-modeling block represents the floor plan as a mesh of 2-D grid points and produces a mapping between grid points and the elements of the coefficient matrices  $A_C$ ,  $A_H$ , and  $A_V$ . In Fig. 6, we use  $\mathbf{a}_j$  to denote the  $j$ th column from any coefficient matrices. Note that the mapping in the environment-modeling block only defines the structure of the coefficient matrices, i.e., the correspondences between the  $i$ th grid point and the  $i$ th element in  $\mathbf{a}_j$ . The actual values of these matrices are computed in the observation measure block.

Based on the mapping from camera parameters to the solution vector and the structure of the coefficient matrices, the observation measures of each grid point, given each camera configuration, are calculated to form the coefficient matrices  $A_C$ ,  $A_H$ , and  $A_V$ . These coefficient matrices are, in turn, used to construct the objective function in the optimization stage.

In the optimization stage, the optimal solution  $\mathbf{x}$  is searched under the guidance of the objective function  $F = \sum_i c_i$ . There exist multiple local maxima because of the complex interaction among multiple cameras; thus, a global optimizer is recommended. Gradient-based optimization approaches, including the Newton and Quasi-Newton methods, are not employed due to the difficulties in computing or estimating the gradient of the objective functions in (17) and (18). In comparison with gradient-based approaches, Monte-Carlo optimization methods are more suitable for our problems. Monte-Carlo methods can find the optimal solution without explicit computations of the gradient of the objective function. In addition, Monte-Carlo methods are powerful when dealing with large-dimensional vectors and local maxima. Simulated annealing and generic algorithm are two popular Monte-Carlo methods. David *et al.* exploited the genetic algorithm to implement Erdem and Scalorff's algorithm [12]. Simulated annealing also finds applications in the optimization of sensor placement [11]. In the following discussion, the genetic algorithm is employed. Another reason that we have selected the genetic algorithm lies in the fact that the solution vector is readily binary.

The search for the optimal solution starts with initialization. Following the conventions of the generic algorithm, the initial pool of chromosomes  $\{\mathbf{x}_k^{(o)}\}$  is generated, where  $k$  denotes the  $k$ th chromosome in the population. Reproduction is carried out, including operations such as selection, crossover, mutation, and elitism, to form the next generation. The newly constructed objective function is employed to evaluate the fitness of each

TABLE I  
LIST OF VARIABLES USED IN THE PROPOSED ALGORITHM

| Index | Block                | Variables  | User specified     | Automatically computed | Dependent variable |             |
|-------|----------------------|--|--------------------|------------------------|--------------------|-------------|
| 1     | Environment modeling | 2D floor plan + height information                   | √                  |                        |                    |             |
| 2     |                      | Path layout and orientation                          | √                  |                        |                    |             |
| 3     |                      | 3D information of obstacles                          | √                  |                        |                    |             |
| 4     | Camera modeling      | Camera type  | √                  | √                      | 1                  |             |
| 5     |                      | Camera extrinsic parameters: range and sampling rate | √                  | √                      | 1                  |             |
| 6     |                      | Camera intrinsic parameters: range and sampling rate | √                  | √                      | 1                  |             |
| 7     | Observation measure  | $\alpha_R$ and $\alpha_D$                            |                    | √                      | 6                  |             |
| 8     |                      | $w_R$ and $w_D$                                      | √                  | √                      | Default            |             |
| 9     | Objective function   | $Q_F$ and $Q_T$                                      | √                  | √                      | 1 and 6            |             |
| 10    |                      | $w_C$ , $w_H$ , and $w_V$                            | √                  | √                      | 1, 5, and 6        |             |
| 11    |                      | Constraints  | $M_{R,o,i}$        | √                      | √                  | 1           |
| 12    |                      |  | $w_R$ and $w_{FV}$ | √                      | √                  | 1, 5, and 6 |
| 13    | Optimization         | Initial population                                   | √                  | √                      | Default            |             |
| 14    |                      | Crossover method, mutation rate, and elitism rate    | √                  | √                      | Default            |             |
| 15    |                      | Stopping criterion                                   | √                  | √                      | Default            |             |

chromosome in the population. The reproduction and evaluation process iterates until the stopping criteria are satisfied. In Fig. 6,  $\{\mathbf{x}_k^{(Iter)}\}$  represents the population at the  $(Iter)$ th iteration. In the end, the optimal parameters are obtained based on the mapping between the optimal solution  $\mathbf{x}^*$  and camera configurations.

Optimization accounts for the majority of the computational complexity, which heavily depends on camera-related quantities (e.g., the number of cameras, the feasible range of the camera parameters, and the sampling rate of the camera parameters) and environment-related quantities (e.g., the scale of the environment and the sampling rate of the grid points). Path constraints and occlusions are established in the preparation stage; thus, the additionally induced computations are not as significant as the aforementioned quantities.

Preparation and optimization are automatically implemented, given the necessary information of the environments. Fig. 6 emulates the necessary inputs for each modeling block. In our implementation, some of the camera parameters can automatically be derived from environment modeling if they are not specified otherwise. To clearly illustrate the additional computation or information needed as the necessary input to our algorithm, Table I lists the variables used in the proposed algorithm. In our implementation, the only necessary input is a 2-D floor plan with information about the obstacles/paths that need to be considered. A 3-D CAD model of the environment is a promising input format. The floor plan is modeled as a polygon; thus, one alternative approach is to list the coordinates of the vertices of the floor plan and the obstacles/paths in a text file. Our implementation adopts the second approach. Other variables can either be computed from given information or use default values. Table I also lists the dependency between variables. For example, the cameras' extrinsic parameters can be derived from the 3-D model of the floor plan.

## VII. EXPERIMENTAL RESULTS

We begin this section with the discussion regarding the selection of parameters in the definition of the observation

measure and the construction of the objective function. We then introduce our experimental methodology and validate the newly developed observation measure for different types of cameras. Our experimental results, using two floor plans, are presented and compared with a reference algorithm that was proposed by Erdem and Sclaroff [15]. Three criteria are used to evaluate and compare the performances of various algorithms: 1) coverage; 2) handoff success rate; and 3) frontal-view percentage. The handoff success rate denotes the ratio between the number of successful handoffs and the total number of handoff requests. The frontal-view percentage is given by the ratio between the number of frames with required orientations of the object of interest and the total number of frames with the object of interest being tracked. Comparing Erdem and Sclaroff's method with our proposed method, an improved handoff success rate is expected. When the path constraint is imposed, an improved frontal-view percentage is also expected.

### A. Parameter Selection

There are two sets of parameters: 1) normalization coefficients ( $\alpha_R$  and  $\alpha_D$ ) and 2) importance weights ( $w_R$ ,  $w_D$ ,  $w_C$ ,  $w_H$ ,  $w_V$ ,  $w_R$ , and  $w_{FV}$ ). The goal of choosing the appropriate normalization coefficients is to provide a uniform comparison basis for different types of cameras and cameras with various intrinsic and extrinsic parameters. In so doing, sensor planning and camera handoff can be conducted independent of the actual types of cameras that were selected. In general, we normalize the  $M_R$  and  $M_D$  components in the range of [0, 1].

For static-perspective cameras, the maximum of  $M_R$  is achieved at  $\hat{z}' = -T_Z / \tan \theta_T$ . We have  $M_{R,\max} = \alpha_R / \hat{z}' |_{\hat{z}' = -T_Z / \tan \theta_T} = 1$  and thus,  $\alpha_R = -T_Z / \tan \theta_T$ . To normalize the  $M_D$  component, we need  $\alpha_D = 0.5$ . For omnidirectional cameras, the maximum of the  $M_R$  component is obtained by letting  $\theta = 0$ :  $M_{R,\max} = \alpha_R f \lambda_{\theta,1} / Z$ . In consequence, we arrive at  $\alpha_R = Z / f \lambda_{\theta,1}$ . In a similar fashion, we set  $\alpha_D = 1$  to normalize the  $M_D$  component for omnidirectional cameras.

Unlike the selection of the normalization coefficients, which depends on the characteristics of the cameras used, the

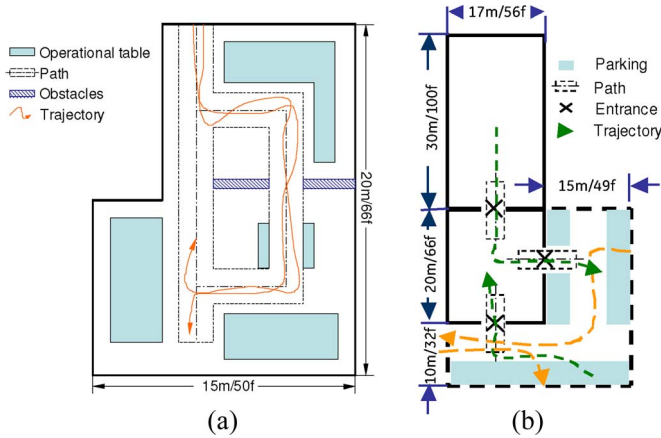


Fig. 7. Tested floor plans: (a) an office floor plan with path constraints and (b) a floor plan with mixed indoor and outdoor environments. These two floor plans are referred to as plan A and B, respectively.

selection of the importance weights is application dependent. We purposefully reserve the freedom for users to choose different importance weights according to their special requirements to increase our algorithm's flexibility. Meanwhile, default values can be used if the corresponding variables are not specified by users. The default values of  $w_R$  and  $w_D$  are simply 0.5. We could compute  $w_C$ ,  $w_H$ , and  $w_V$  such that the turning point of the objective function is placed at the middle point between the contours defined by  $Q_T$  and  $Q_F$ . The weights  $w_R(w_{FV})$  can be calculated as the ratio between the area of the floor plan and the area of the grid points that require special resolution (orientation). In the following experiments, the importance weights are set to default values.

### B. Experimental Methodology

The floor plans used in this section are shown in Fig. 7. Fig. 7(a) illustrates an environment with a predefined path where workers proceed in a predefined sequence. One floor plan with mixed indoor and outdoor environments is used to examine the flexibility of the proposed algorithms. In the following experiments, we refer to these plans as plans A and B. These floor plans are deliberately selected to cover a large variety of environments that are encountered in practical surveillance.

The selected floor plans are used to test various aspects of the proposed algorithm according to their characteristics. The scale of indoor environments, e.g., floor plan A, is relatively small. Those test beds are only used to verify the performance of the proposed camera-placement algorithm based on cameras with smaller FOVs, e.g., static-perspective and omnidirectional cameras. PTZ cameras that are equipped with significantly larger FOVs appear to be more appropriate for large-scale surveillance. Therefore, floor plan B is tested using PTZ cameras. In addition, a predefined path is given in floor plan A, and preferred observation directions are specified for entrance areas in floor plan B. Path constraints are imposed to test whether an improved frontal-view percentage can be achieved. Static-perspective cameras are placed along the walls of the environment, whereas omnidirectional and PTZ cameras can be mounted either on the ceiling or along the walls at sampled grid points, with an interval of 1 m.

To obtain a statistically valid estimation of the handoff success rate, simulations are carried out to enable a large amount of tests under various conditions [19]. A pedestrian behavior simulator [4], [32] is implemented so that we can achieve a close resemblance to experiments in real environments and, in turn, an accurate estimation of the handoff success rate. Interested readers can refer to the original papers for details. In our experiments, the arrival of the pedestrian follows a Poisson distribution, with an average arrival rate of 0.01 person/s. The average walking speed is 0.5 m/s. Several points of interest are randomly generated to form a pedestrian trace. Fig. 7 also depicts some randomly generated pedestrian traces. The handoff success rate and the frontal-view percentage are obtained from simulation results of 300 randomly generated traces.

### C. Experiment on Observation Measures

In the following experiment, a static-perspective camera is placed at  $T_C = [0 \ 0 \ 3 \text{ m}]^T$ , which looks down toward the ground plane at a tilt angle of  $-30^\circ$ . Its pan angle is set to zero. The image size is  $640 \times 480$ . The focal length of the camera is 21.0 mm. Points are uniformly sampled on the ground plane ( $Z = 0$ ), with  $X$  being in the range of  $-8$  m to  $8$  m and  $Y$  in the range of  $2$  m to  $10$  m. Based on these parameters, the normalization coefficient of the  $M_R$  component is  $\alpha_R = -3/\tan(-30^\circ) = 5.2$ . As we have previously mentioned, a smaller decreasing/increasing rate of the  $M_D$  component is desired when the target is at a long distance. In our implementation, we choose

$$\begin{cases} \beta_1 |T_Z / \tan \theta_T| + \beta_o = 1 \\ 2\beta_1 |T_Z / \tan \theta_T| + \beta_o = 0.5 \end{cases}$$

and obtain  $\beta_1 = -0.1$  and  $\beta_o = 1.5$ . In summary, the parameters used are listed as follows:  $\alpha_R = 5.2$ ,  $\alpha_D = 0.5$ ,  $\beta_1 = -0.1$ ,  $\beta_o = 1.5$ ,  $w_R = 0.25$ , and  $w_D = 0.75$ .

Fig. 8 shows the observation measure for the perspective camera. As expected, in Fig. 8(a)–(c),  $M_R$  increases as the target moves toward the camera along the optical axis, and  $M_D$  increases as the target moves toward the image center. Based on Fig. 8(d), the best observation area with the maximum observation measure is in the proximity of  $[0 \ 5 \text{ m} \ 0]^T$ . As the object moves from this area, the observation measure decreases. A higher penalty is given to the motion along the  $x$ -axis, i.e., the direction orthogonal to the optical axis of the camera. The proposed observation measure gives a quantified evaluation of the tracking and observation suitability, which also agrees with our intuition and visual inspection.

In the second simulation, an omnidirectional camera that follows the equidistance projection model is placed at  $T_C = [0 \ 0 \ 3 \text{ m}]^T$ , which overlooks an area with  $(X, Y)$  in the range of  $-6$  m to  $6$  m. The image size is  $640 \times 640$ . The normalization coefficient for the resolution component is given by  $\alpha_R = 6/640 = 9.4 \times 10^{-3}$ . Other parameters that were used are listed as follows:  $\alpha_D = 1$ ,  $w_R = 0.25$ , and  $w_D = 0.75$ . The resulting observation measure is shown in Fig. 9. A radially symmetric shape is obtained, which agrees with the characteristics of an omnidirectional camera.

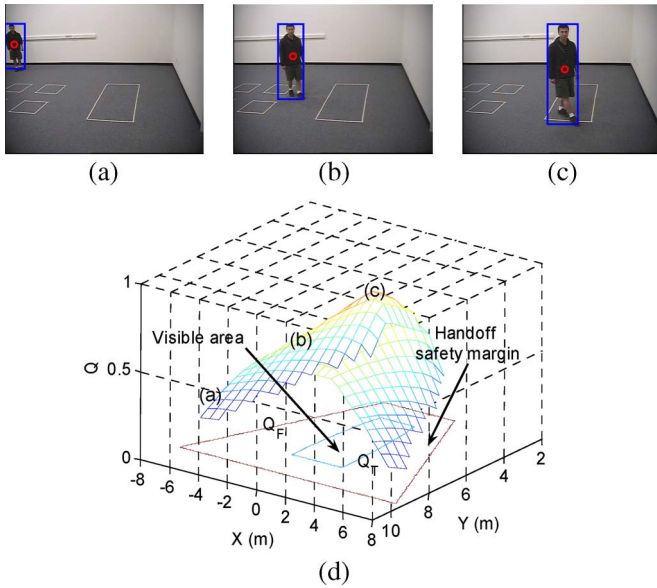


Fig. 8. (a)–(c) Sample frames from a perspective camera with the target at different positions. The blue rectangle and the red circle highlight the bounding box and the centroid of the detected target, respectively. The estimated resolution components  $M_R$  are given as follows: (a) 0.16; (b) 0.57; and (c) 0.76. The estimated distance components  $M_D$  are given as follows: (a) 0.11; (b) 0.40; and (c) 0.77. (d) Graphical illustration of the observation measure and handoff safety margin for a perspective camera. The positions of the sample frames are specified.

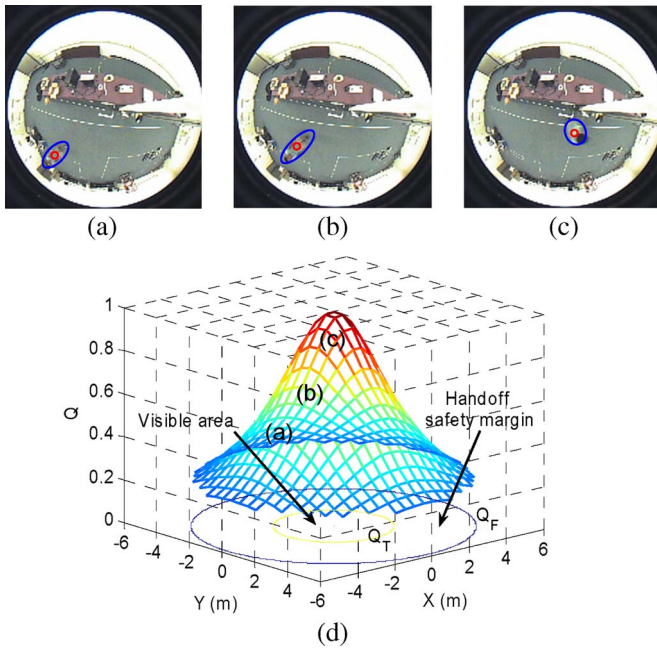


Fig. 9. (a)–(c) Sample frames from an omnidirectional camera with the target at different radial distances. The blue ellipse and the red circle highlight the area and the centroid of the detected target, respectively. The estimated resolution components  $M_R$  are given as follows: (a) 0.57; (b) 0.70; and (c) 0.91. The estimated distance components  $M_D$  are given as follows: (a) 0.26; (b) 0.41; and (c) 0.71. (d) Graphical illustration of the observation measure and handoff safety margin for an omnidirectional camera. The positions of the sample frames are specified.

#### D. Experiment on Sensor Planning

In the following experiments,  $w_C$ ,  $w_H$ , and  $w_V$  are set to 1, 2, and 5, respectively. The failure and trigger thresholds are 0 and 0.6, respectively. For floor plan A, the required visible

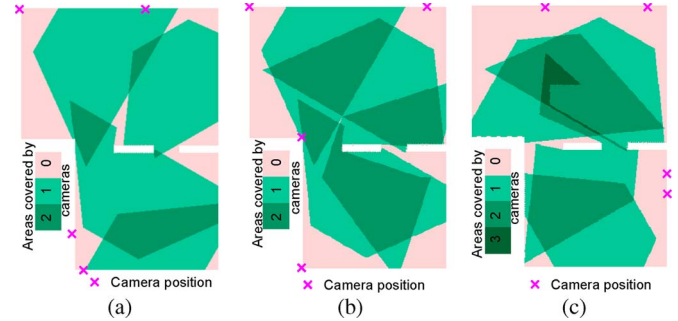


Fig. 10. Optimal camera positioning of floor plan A for the Max-Coverage problem using perspective cameras. (a) Erdem and Sclaroff's method (the coverage is 84.8%, the handoff success rate is 6.0%, and the frontal view percentage is 67.7%). (b) Our method (the coverage is 74.7%, the handoff success rate is 56.9%, and the frontal view percentage is 28.7%). (c) Our method with path constraint (the coverage is 72.1%, the handoff success rate is 58.0%, and frontal view percentage is 93.5%).

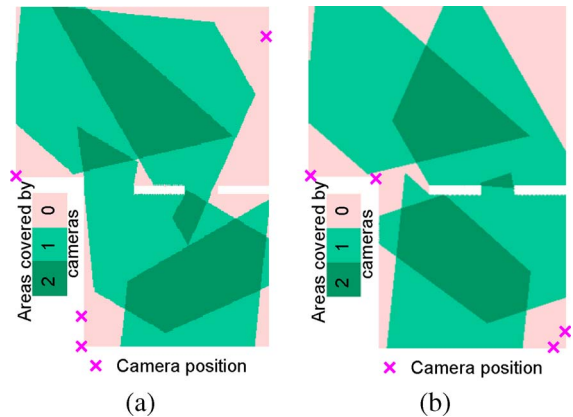


Fig. 11. Optimal camera positioning of floor plan A for the Min-Cost problem using perspective cameras (coverage  $\geq 80\%$ ). (a) Our method (the coverage is 81.3%, the handoff success rate is 43.7%, and the frontal view percentage is 41.0%). (b) Our method with path constraint (the coverage is 81.6%, the handoff success rate is 47.1%, and the frontal view percentage is 69.0%).

distance is about 10 m, and the height is 3 m; thus, the same pair of tilt angle and focal length can be used for static-perspective cameras, with  $f = 21.0$  mm and  $\theta_T = -30^\circ$ .

Fig. 10 illustrates the experimental results for floor plan A by using static-perspective cameras to solve the Max-Coverage problem. Our approach chooses a camera-positioning scheme with a slightly decreased coverage from 84.8% to 74.7% compared to Erdem and Sclaroff's method. However, the handoff success rate is substantially improved from 6.0% to 56.9%. In addition, we add the frontal-view criterion with  $w_{FV} = 5$ . The frontal-view percentage is elevated from 28.7% to 93.5%. Based on Fig. 10(b) and (c), we could see that the cameras are oriented toward the direction of the predefined path after introducing the path constraint.

The Min-Cost problem imposes additional requirements on the overall coverage, which leaves less freedom in optimization to achieve the maximum handoff success rate. As Fig. 11 demonstrates, the overall coverage is constrained to be above 80%. With similar coverage (Erdem and Sclaroff's method has 84.8%, whereas our method has 81.3%), our algorithm can achieve a much higher handoff success rate (i.e., 43.7%) than the conventional approach (i.e., 6.0%).

Fig. 12 demonstrates the experimental results for PTZ cameras. The handoff success rate is elevated from 48.7% to

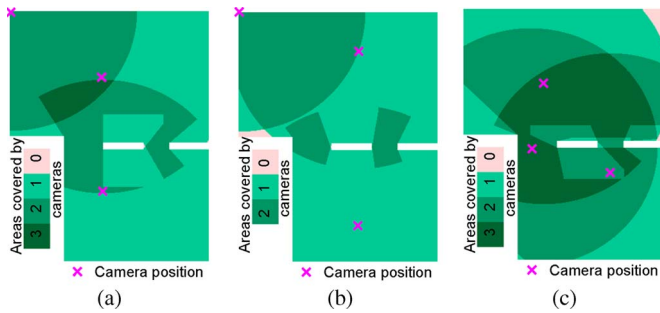


Fig. 12. Optimal camera positioning of floor plan A for the Max-Coverage problem using PTZ cameras. (a) Erdem and Sclaroff's method (the coverage is 100.0%, the handoff success rate is 48.7%, and the frontal view percentage is 52.5%). (b) Our method (the coverage is 99.5%, the handoff success rate is 100.0%, and the frontal view percentage is 53.4%). (c) Our method with path constraint (the coverage is 99.0%, the handoff success rate is 100.0%, and the frontal view percentage is 71.1%).

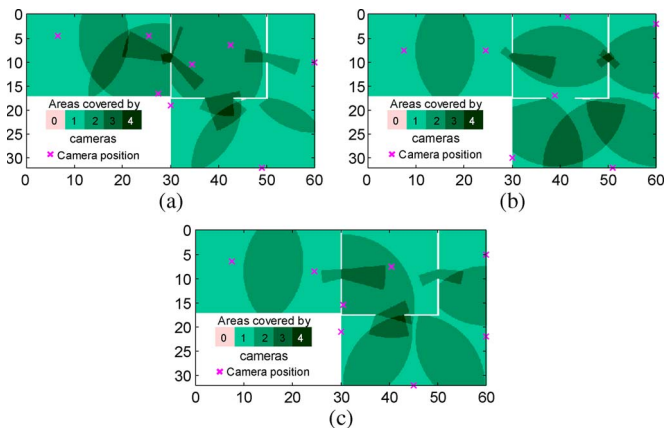


Fig. 13. Optimal camera positioning of floor plan B for the Max-Coverage problem using PTZ cameras. (a) Erdem and Sclaroff's method (the coverage is 100.0%, the handoff success rate is 71.6%, and the frontal view percentage is 56.2%). (b) Our method (the coverage is 100.0%, the handoff success rate is 92.8%, and the frontal view percentage is 42.4%). (c) Our method with path constraint (the coverage is 100.0%, the handoff success rate is 91.5%, and the frontal view percentage is 94.2%).

100% but at the cost of a marginal decrease in coverage from 100.0% to 99.5% when comparing the performance of the reference method [15] and the proposed method for floor plan A. A similar performance improvement is achieved for floor plan B, which is an example with mixed indoor and outdoor environments, as shown in Fig. 13. Our algorithm enhances the handoff success rate from 71.6% to 92.8% while maintaining the same coverage of 100.0% in comparison with the reference algorithm. To obtain frontal-view observations at entrance areas, path constraints are imposed, which results in an improvement in frontal-view percentage from 56.2% of the reference algorithm to 94.2%.

In parallel, experiments are conducted using omnidirectional cameras. To cover a radius of 6 m at a height of 3 m, the chosen focal length is 15.4 mm. Fig. 14 shows the optimal camera placement. At the cost of a 10.6% decrease in coverage, the handoff success rate increases from 50.0% to 92.6% for floor plan A. Unlike perspective cameras that can look into a particular direction for a frontal view of the target, omnidirectional cameras have a  $360^\circ \times 90^\circ$  view. Therefore, the improvement in frontal-view percentage from imposing the path constraint

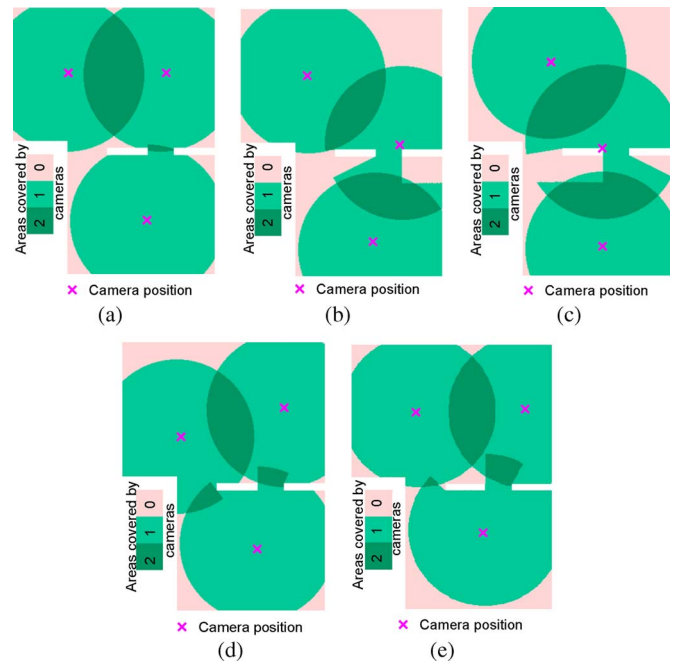


Fig. 14. Optimal camera positioning of floor plan A using omnidirectional cameras. The Max-Coverage problem: (a) Erdem and Sclaroff's method (the coverage is 92.1%, the handoff success rate is 50.0%, and the frontal view percentage is 49.9%), (b) our method (the coverage is 81.5%, the handoff success rate is 92.6%, and the frontal view percentage is 53.4%), and (c) our method with path constraint (the coverage is 80.0%, the handoff success rate is 100.0%, and the frontal view percentage is 57.6%). The Min-Cost problem (coverage  $\geq 90\%$ ): (d) our method (the coverage is 91.2%, the handoff success rate is 52.2%, and the frontal view percentage is 45.7%) and (e) our method with path constraint (the coverage is 90.7%, the handoff success rate is 100.0%, and the frontal view percentage is 53.4%).

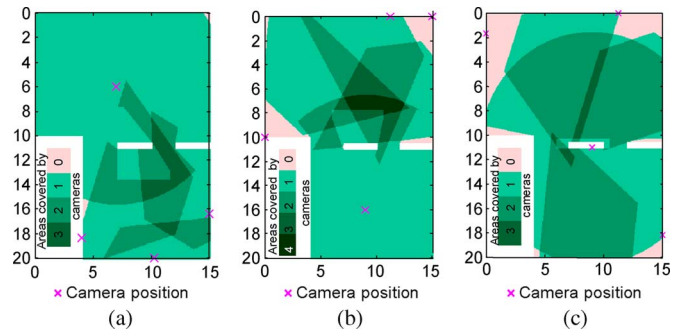


Fig. 15. Optimal camera positioning of floor plan A for the Max-Coverage problem using perspective and PTZ cameras. (a) Erdem and Sclaroff's method (the coverage is 99.7%, the handoff success rate is 44.7%, and the frontal view percentage is 40.4%). (b) Our method (the coverage is 95.1%, the handoff success rate is 100.0%, and the frontal view percentage is 63.1%). (c) Our method with path constraint (the coverage is 91.6%, the handoff success rate is 100.0%, and the frontal view percentage is 90.9%).

is not substantial, which was indicated by a slight increase of 4.2%.

As we have mentioned in Section VII-A, appropriate normalization coefficients are selected to provide a uniform comparison basis for different types of cameras and cameras with various intrinsic and extrinsic parameters so that the proposed sensor-planning algorithm is applicable to systems with heterogeneous cameras. Fig. 15 demonstrates the experimental results based on floor plan A, where two types of cameras—static perspective and PTZ—are deployed into the environment. In

TABLE II  
SYSTEM PERFORMANCE COMPARISON

| Floor plan A (20m×15m)          |                         |                                 |          |                      |                         |                                 |
|---------------------------------|-------------------------|---------------------------------|----------|----------------------|-------------------------|---------------------------------|
|                                 | Problem                 | Method                          | Coverage | Handoff success rate | Frontal view percentage | $\frac{\Delta HSR}{ \Delta C }$ |
| Perspective                     | Max-Coverage            | Erdem & Sclaroff                | 84.8     | 6.0                  | 67.7                    |                                 |
|                                 |                         | Our method                      | 74.7     | 56.9                 | 28.7                    | <b>5.0</b>                      |
|                                 |                         | Our method with path constraint | 72.1     | 58.0                 | 93.5                    | <b>4.1</b>                      |
|                                 | Min-Cost (Coverage>80%) | Our method                      | 81.3     | 43.7                 | 41.0                    | <b>10.8</b>                     |
| Our method with path constraint |                         | 81.6                            | 47.1     | 69.0                 | <b>12.8</b>             |                                 |
| Omnidirectional                 | Max-Coverage            | Erdem & Sclaroff                | 92.1     | 50.0                 | 49.9                    |                                 |
|                                 |                         | Our method                      | 81.5     | 92.6                 | 53.4                    | <b>4.0</b>                      |
|                                 |                         | Our method with path constraint | 80.0     | 100.0                | 57.6                    | <b>4.1</b>                      |
|                                 | Min-Cost (Coverage>90%) | Our method                      | 91.2     | 52.2                 | 45.7                    | <b>2.4</b>                      |
| Our method with path constraint |                         | 90.7                            | 100.0    | 53.4                 | <b>35.7</b>             |                                 |
| PTZ                             | Max-Coverage            | Erdem & Sclaroff                | 100.0    | 48.7                 | 52.5                    |                                 |
|                                 |                         | Our method                      | 99.5     | 100.0                | 53.4                    | <b>102.6</b>                    |
|                                 |                         | Our method with path constraint | 99.0     | 100.0                | 71.1                    | <b>51.3</b>                     |
| Pers. & PTZ                     | Max-Coverage            | Erdem & Sclaroff                | 99.7     | 44.7                 | 40.4                    |                                 |
|                                 |                         | Our method                      | 95.1     | 100.0                | 63.1                    | <b>12.0</b>                     |
|                                 |                         | Our method with path constraint | 91.6     | 100.0                | 90.9                    | <b>6.8</b>                      |
| Floor plan B (60m×30m)          |                         |                                 |          |                      |                         |                                 |
|                                 | Problem                 | Method                          | Coverage | Handoff success rate | Frontal view percentage | $\Delta HSR$                    |
| PTZ                             | Max-Coverage            | Erdem & Sclaroff                | 100.0    | 71.6                 | 56.2                    |                                 |
|                                 |                         | Our method                      | 100.0    | 92.8                 | 42.4                    | <b>21.2</b>                     |
|                                 |                         | Our method with path constraint | 100.0    | 91.5                 | 94.2                    | <b>19.9</b>                     |

TABLE III  
PROCESSING TIME COMPARISON

| Floor plan | Dimensions | Number of cameras | Type of problem | Processing time (minutes) |                  |            |
|------------|------------|-------------------|-----------------|---------------------------|------------------|------------|
|            |            |                   |                 | Preparation               | Optimization     |            |
|            |            |                   |                 |                           | Erdem & Sclaroff | Our method |
| A          | 20m×15m    | 3                 | Max-Coverage    | < 1                       | <5               | <5         |
|            |            |                   | Min-cost        |                           | <5               | <5         |
| B          | 60m×30m    | 8                 | Max-Coverage    | <2                        | 30-45            | 30-45      |
|            |            |                   | Min-cost        |                           | 5-10             | 35-60      |

comparison with Erdem and Sclaroff's method, our algorithm achieves a significant improvement in the handoff success rate (i.e., 100.0% versus 44.7%) and a considerably increased frontal-view percentage (i.e., 90.9% versus 40.4%) once the path constraint is imposed. Compared to the experimental results using static-perspective cameras in Fig. 10, the camera placement with heterogeneous cameras produces higher coverage and handoff success rate, at the cost of decrease in frontal-view percentage. On the contrary, compared to the experimental results using PTZ cameras in Fig. 12, systems with heterogeneous cameras feature a higher frontal-view percentage, at the cost of degradation in coverage and handoff success rate. The aforementioned observation agrees with the characteristics of static-perspective and PTZ cameras. In comparison with PTZ cameras, static-perspective cameras, with a smaller FOV, look into a specific direction, which facilitates the definition of frontal-view directions. Therefore, with similar system complexity, the use of heterogeneous cameras can explore the advantages of different types of cameras and achieve a better

balance between coverage/handoff success rate and frontal-view percentage.

### E. Performance Comparisons

Table II summarizes the performance comparison between the proposed algorithm and the reference algorithm described by Erdem and Sclaroff [15]. Consistent observations are obtained from experiments using two floor plans and three types of cameras. Compared to the reference algorithm, our algorithms produce considerably improved handoff success rate and frontal-view percentage but at the cost of slightly decreased coverage. This amount of decrease in coverage is inevitable to maintain overlapped FOVs between adjacent cameras required by continuous and automated tracking, given a fixed number of cameras. The ratio between the increase in handoff success rate and the decrease in coverage  $\Delta HSR/|\Delta C|$  describes the advantage of our algorithms. For the Max-Coverage problem, every 1% decrease in coverage results in a 4%–10% increase

in the handoff success rate. An even higher improvement rate can be achieved for the Min-Cost problem. The efficiency of the proposed algorithms in balancing the overall coverage and sufficient overlapped FOVs becomes evident. Furthermore, our algorithms can also handle additional constraints, e.g., the frontal-view requirement. The resulting algorithms are able to maintain a similar improvement rate in the handoff success rate with further improved frontal-view percentage.

The conventional sensor-planning methods achieve a camera placement with a maximized coverage. In such a system, although the target is visible, it cannot consistently be labeled or recognized as the same identity across different cameras because of handoff failures that result from insufficient overlapped FOVs. The corresponding camera placement cannot support automated persistent surveillance, because the tracked or identified target trajectories are disjoint at the junction areas of adjacent cameras. In contrast, our sensor placement ensures a continuous consistently labeled trajectory. The slightly decreased coverage can easily be compensated for by adding an additional camera. The cost of an extra camera is acceptable in comparison with a system with inherent weakness in persistent and continuous tracking.

Finally, we compare the computational complexity between the proposed and reference algorithms. The objective function of the proposed algorithm is nonlinear for both Max-Coverage and Min-Cost problems. As for the reference algorithm, the Min-Cost problem can be solved via linear programming. Nevertheless, the objective function for the Max-Coverage problem is also nonlinear. Therefore, our algorithm has similar computational complexity as the reference algorithm in solving the Max-Coverage problem. As we have previously mentioned, our algorithm for the Min-Cost problem is a sequential process. The computational complexity of the first step is similar to that of the reference algorithm. Additional computations come from the second step, which has a nonlinear objective function. Table III summarizes the dimensions of the floor plan, the number of cameras deployed, and the processing time for the preparation and optimization stages. Algorithms are implemented in Matlab and run on a personal computer with dual 1.6-GHz CPUs and 1-GB RAM. According to our experiments, we observe that, for environments with small scales, our algorithms require similar processing time as the reference methods for solving both Max-Coverage and Min-Cost problems. As the environment scale increases, our algorithms start to require noticeably increased computations for solving the Min-Cost problem. Compared to the advantage of continuously and consistently maintaining a target's trajectory in real-time surveillance, the increased computational complexity in offline processing is acceptable.

### VIII. CONCLUSION

In this paper, we have proposed a sensor positioning algorithm for various types of cameras in the context of persistent and automated tracking and improved existing algorithms by incorporating handoff rate analysis with coverage and visibility analysis. Direct constraint and adaptive weight approaches were derived from the general method to solve the resolution and frontal-view constraints. Significantly improved handoff success rate and frontal-view percentage were reported via

experiments and comparisons with a reference algorithm based on typical indoor and outdoor floor plans of various scales. These experimental results indicate the efficiency of the proposed algorithm in balancing the overall coverage and sufficient overlapped FOVs. With considerably improved handoff success rate and frontal-view percentage, the proposed algorithm produces robust and enhanced performance compared to the reference algorithm presented in the work of Erdem and Sclaroff when applied to automated tracking systems.

### REFERENCES

- [1] B. Abidi, N. Aragam, Y. Yao, and M. Abidi, "Survey and analysis of multimodel sensor planning and integration for wide area surveillance," *ACM Comput. Surv.*, vol. 41, no. 1, pp. 1–36, Dec. 2008.
- [2] H. M. Ammari and S. K. Das, "Promoting heterogeneity, mobility, and energy-aware Voronoi diagram in wireless sensor networks," *IEEE Trans. Parallel Distrib. Syst.*, vol. 19, no. 7, pp. 995–1008, Jul. 2008.
- [3] F. Angella, L. Reithler, and F. Galesio, "Optimal deployment of cameras for video surveillance systems," in *IEEE Int. Conf. Adv. Video Signal Based Surveillance*, London, U.K., Sep. 2007, pp. 388–392.
- [4] G. Antonini, S. Venegas, M. Bierlaire, and J. Thiran, "Behavioral priors for detection and tracking of pedestrians in video sequences," *Int. J. Comput. Vis.*, vol. 69, no. 2, pp. 159–180, Aug. 2006.
- [5] R. Bodor, P. Schrater, and N. Papanikolopoulos, "Multicamera positioning to optimize task observability," in *IEEE Conf. Adv. Video Signal Based Surveillance*, Como, Italy, Sep. 2005, pp. 552–557.
- [6] T. E. Boulton, X. Gao, R. Micheals, and M. Eckmann, "Omnidirectional visual surveillance," *Image Vis. Comput.*, vol. 22, no. 7, pp. 515–534, Jul. 2004.
- [7] Q. Cai and J. K. Aggarwal, "Tracking human motion in structured environments using a distributed-camera system," *IEEE Trans. Pattern Anal. Mach. Intell.*, vol. 21, no. 11, pp. 1241–1247, Nov. 1999.
- [8] S. Chen, Y. Li, J. Zhang, and W. Wang, *Active Sensor Planning for Multiview Vision Tasks*. New York: Springer-Verlag, 2008.
- [9] S. Y. Chen and Y. F. Li, "Automatic sensor placement for model-based robot vision," *IEEE Trans. Syst., Man, Cybern. B, Cybern.*, vol. 34, no. 1, pp. 393–408, Feb. 2004.
- [10] X. Chen and J. Davis, "An occlusion metric for selection robust camera configurations," *Mach. Vis. Appl.*, vol. 19, no. 4, pp. 217–222, Jul. 2008.
- [11] P. L. Chiu and F. Y. S. Lin, "A simulated annealing algorithm to support the sensor placement for target location," in *Can. Conf. Elect. Comput. Eng.*, Niagara Falls, ON, Canada, May 2004, pp. 867–870.
- [12] P. David, V. Idasiak, and F. Kratz, "A sensor placement approach for the monitoring of indoor scenes," in *Eur. Conf. Smart Sens. Context*, Kendal, U.K., Oct. 2007, pp. 110–125.
- [13] J. W. Davis, A. M. Morison, and D. D. Woods, "An adaptive focus-of-attention model for video surveillance and monitoring," *Mach. Vis. Appl.*, vol. 18, no. 1, pp. 41–64, Feb. 2007.
- [14] E. Dunn, G. Olague, and E. Lutton, "Parisian camera placement for vision metrology," *Pattern Recognit. Lett.*, vol. 27, no. 11, pp. 1209–1219, Aug. 2006.
- [15] U. M. Erdem and S. Sclaroff, "Automated camera layout to satisfy task-specific and floor plan-specific coverage requirements," *Comput. Vis. Image Underst.*, vol. 103, no. 3, pp. 156–169, Sep. 2006.
- [16] L. Fiore, D. Fehr, R. Bodor, A. Drenner, G. Somasundaram, and N. Papanikolopoulos, "Multicamera human activity monitoring," *J. Intell. Robot. Syst.*, vol. 52, no. 1, pp. 5–43, May 2008.
- [17] Z. Guo, M. Zhuo, and G. Jiang, "Adaptive sensor placement and boundary estimation for monitoring mass objects," *IEEE Trans. Syst., Man, Cybern. B, Cybern.*, vol. 38, no. 1, pp. 222–232, Feb. 2008.
- [18] A. Gupta, A. Mittal, and L. S. Davis, "COST: An approach for camera selection and multiobject inference ordering in dynamic scenes," in *IEEE Int. Conf. Comput. Vis.*, Rio de Janeiro, Brazil, Oct. 2007, pp. 1–8.
- [19] L. Hodge and M. Kamel, "A simulation environment for multisensor planning," *Simulation*, vol. 76, no. 6, pp. 371–380, Jun. 2001.
- [20] E. Horster and R. Lienhart, "On the optimal placement of multiple visual sensors," in *ACM Int. Workshop Video Surveillance Sensor Netw.*, Santa Barbara, CA, Oct. 2006, pp. 111–120.
- [21] W. Hu, T. Tan, L. Wang, and S. Maybank, "A survey on visual surveillance of object motion and behaviors," *IEEE Trans. Syst., Man, Cybern. C, Appl. Rev.*, vol. 34, no. 3, pp. 334–352, Aug. 2004.

- [22] V. Isler, S. Kannan, and K. Daniilidis, "VC-dimension of exterior visibility," *IEEE Trans. Pattern Anal. Mach. Intell.*, vol. 26, no. 5, pp. 667–671, May 2004.
- [23] V. Isler, S. Khanna, J. Spletzer, and C. J. Taylor, "Target tracking with distributed sensors: The focus of attention problem," *Comput. Vis. Image Underst.*, vol. 100, no. 1/2, pp. 225–247, Oct./Nov. 2005.
- [24] J. Kannala and S. Brandt, "A generic camera calibration method for fish-eye lenses," in *Int. Conf. Pattern Recog.*, Cambridge, U.K., Aug. 2004, pp. 10–13.
- [25] S. Khan and M. Shah, "Consistent labeling of tracked objects in multiple cameras with overlapping fields of view," *IEEE Trans. Pattern Anal. Mach. Intell.*, vol. 25, no. 10, pp. 1355–1360, Oct. 2003.
- [26] A. Krause, C. Guestrin, A. Gupta, and J. Kleinberg, "Near-optimal sensor placements: Maximizing information while minimizing communication cost," in *Int. Conf. Inf. Process. Sensor Netw.*, Nashville, TN, Apr. 2006, pp. 2–10.
- [27] A. Krause, A. Singh, and C. Guestrin, "Near-optimal sensor placements in Gaussian processes: Theory, efficient algorithms, and empirical studies," *J. Mach. Learn. Res.*, vol. 9, pp. 235–284, Feb. 2008.
- [28] J. Lee, "Analyses of visibility sites on topographic surfaces," *Int. J. Geogr. Inf. Syst.*, vol. 5, no. 4, pp. 413–429, Oct.–Dec. 1991.
- [29] M. Ma and Y. Yang, "Adaptive triangular deployment algorithm for unattended mobile sensor networks," *IEEE Trans. Comput.*, vol. 56, no. 7, pp. 946–958, Jul. 2007.
- [30] A. Mittal and L. S. Davis, "Visibility analysis and sensor planning in dynamic environments," in *Eur. Conf. Comput. Vis.*, Prague, Czech Republic, May 2004, pp. 175–189.
- [31] J. O'Rourke, *Art Gallery Theorems and Algorithms*. New York: Oxford Univ. Press, 1987.
- [32] J. Pettre, T. Simeon, and J. P. Laumond, "Planning human walk in virtual environments," in *IEEE/RSJ Int. Conf. Intell. Robots Syst.*, Lausanne, Switzerland, Sep. 2002, pp. 3048–3053.
- [33] P. J. Phillips, H. Moon, S. A. Rizvi, and P. J. Rauss, "The FERET evaluation methodology for face recognition algorithms," *IEEE Trans. Pattern Anal. Mach. Intell.*, vol. 22, no. 10, pp. 1090–1103, Oct. 2000.
- [34] F. Z. Quereshi and D. Teropoulos, "Towards intelligent camera networks: A virtual vision approach," in *IEEE Int. Workshop Visual Surveillance Perform. Eval. Tracking Surveillance*, Beijing, China, Oct. 2005, pp. 177–184.
- [35] S. Ram, K. R. Ramakrishnan, P. K. Atrey, V. K. Singh, and M. S. Kankanalli, "A design methodology for selection and placement of sensors in multimedia surveillance systems," in *ACM Int. Workshop Video Surveillance Sensor Netw.*, Santa Barbara, CA, Oct. 2006, pp. 121–130.
- [36] S. D. Roy, S. Chaudhury, and S. Banerjee, "Active recognition through next view planning: A survey," *Pattern Recognit.*, vol. 37, no. 3, pp. 429–446, Mar. 2004.
- [37] S. D. Roy, S. Chaudhury, and S. Banerjee, "Recognizing large isolated 3-D objects through next view planning using inner camera invariants," *IEEE Trans. Syst., Man, Cybern. B, Cybern.*, vol. 35, no. 2, pp. 282–292, Apr. 2005.
- [38] M. Saadatseresht, F. Samadzadegan, and A. Azizi, "Automatic camera placement in vision metrology based on a fuzzy inference system," *Photogramm. Eng. Remote Sens.*, vol. 71, no. 12, pp. 1375–1385, Dec. 2005.
- [39] K. A. Tarabani, P. K. Allen, and R. Y. Tsai, "A survey of sensor planning in computer vision," *IEEE Trans. Robot. Autom.*, vol. 11, no. 1, pp. 86–104, Feb. 1995.
- [40] I. Tosic and P. Frossard, "Omnidirectional views selection for scene representation," in *IEEE Int. Conf. Image Process.*, Atlanta, GA, Oct. 2006, pp. 2213–2216.
- [41] G. Wang, G. Cao, and T. F. La Porta, "Movement-assisted sensor deployment," *IEEE Trans. Mobile Comput.*, vol. 5, no. 6, pp. 640–652, Jun. 2006.
- [42] L. M. Wong, C. Dumont, and M. A. Abidi, "Next best view system in a 3D object modeling task," in *IEEE Int. Symp. Comput. Intell. Robot. Autom.*, Monterey, CA, Nov. 1999, pp. 306–311.
- [43] C.-H. Wu, K.-C. Lee, and Y.-C. Chung, "A Delaunay triangulation based method for wireless sensor network deployment," in *IEEE Int. Conf. Parallel Distrib. Syst.*, 2006, pp. 253–260.
- [44] S. Yang, M. Li, and J. Wu, "Scan-based movement-assisted sensor deployment methods in wireless sensor networks," *IEEE Trans. Parallel Distrib. Syst.*, vol. 18, no. 8, pp. 1108–1121, Aug. 2007.
- [45] Y. Yao, C.-H. Chen, B. Abidi, D. Page, A. Koschan, and M. Abidi, "Sensor planning for automated and persistent object tracking with multiple cameras," in *IEEE Conf. Comput. Vis. Pattern Recog.*, Anchorage, AK, Jun. 2008, pp. 1–8.
- [46] X. Ying and Z. Hu, "Can we consider central catadioptric cameras and fisheye cameras within a unified imaging model," in *Eur. Conf. Comput. Vis.*, Prague, Czech Republic, May 2004, pp. 442–455.
- [47] S. Yous, N. Ukita, and M. Kidode, "Multiple active camera assignment for high fidelity 3D video," in *IEEE Int. Conf. Comput. Vis. Syst.*, New York, Jan. 2006, p. 43.
- [48] Y. Zou and K. Chakrabarty, "Sensor deployment and target localization in distributed sensor networks," *ACM Trans. Embed. Comput. Syst.*, vol. 2, no. 3, pp. 1–29, Feb. 2003.
- [49] Y. Zou and K. Chakrabarty, "Sensor deployment and target localization based on virtual forces," in *Annu. Joint IEEE INFOCOM*, San Francisco, CA, Mar. 2003, pp. 1293–1303.
- [50] Y. Chen, Z. Wang, and J. Liang, "Automatic dynamic flocking in mobile actuator sensor networks by central Voronoi tessellations," in *IEEE Int. Conf. Mechatronics Autom.*, Niagara Falls, ON, Canada, Jul. 2005, pp. 1630–1635.
- [51] W. Sheng, N. Xi, M. Song, and Y. Chen, "CAD-guided sensor planning for dimensional inspection in automotive manufacturing," *IEEE/ASME Trans. Mechatronics*, vol. 8, no. 3, pp. 372–380, Sep. 2003.



**Yi Yao** received the B.S. and M.S. degrees in electrical engineering from Nanjing University of Aeronautics and Astronautics, Nanjing, China, in 1996 and 2000, respectively, and the Ph.D. degree in electrical engineering from the University of Tennessee, Knoxville, in 2008.

She is currently with the Global Research Center, General Electric. Her research interests include object tracking, sensor planning, and multi-camera surveillance systems.



**Chung-Hao Chen** received the B.S. and M.S. degrees in computer science and information engineering from Fu-Jen University, Taipei, Taiwan, 1997 and 2001, respectively. He is currently a Ph.D. candidate in the Department of Electrical and Computer Engineering, University of Tennessee, Knoxville.

His research interests include object tracking, robotics, and image processing.



**Besma Abidi** (S'88–M'98–SM'06) received the M.S. degree in image processing and remote sensing (with honors) from the National Engineering School of Tunis, Tunisia, and the Ph.D. degree from the University of Tennessee, Knoxville, in 1985, 1986, and 1995, respectively.

She is currently a Research Assistant Professor with the Department of Electrical and Computer Engineering, University of Tennessee. Her research interests include sensor positioning and geometry, video tracking, sensor fusion, nanovision, and biometrics.

Dr. Abidi is a member of the International Society for Optical Engineers, Tau Beta Pi, Eta Kappa Nu, Phi Kappa Phi, and the Order of the Engineer.



**David Page** received the B.S. and M.S. degrees in electrical engineering from Tennessee Technological University, Cookeville, in 1993 and 1995, respectively, and the Ph.D. degree in electrical engineering from the University of Tennessee (UT), Knoxville, in 2003.

After graduation, he was a Civilian Research Engineer with the Naval Surface Warfare Center, Dahlgren, VA. From 2003 to 2008, he was a Research Assistant Professor with the Imaging, Robotics, and Intelligent Systems Laboratory, Department

of Electrical and Computer Engineering, UT. He is currently a partner with Third Dimension Technologies LLC, a Knoxville-based startup. His research interests include 3-D scanning and modeling for computer vision applications, robotic vision systems, and 3-D shape analysis for object description.



**Andreas Koschan** (M'90) received the Diploma (M.S.) degree in computer science and the Dr.-Ing. (Ph.D.) degree in computer engineering from the Technical University Berlin, Berlin, Germany, in 1985 and 1991, respectively.

He is currently a Research Associate Professor with the Department of Electrical and Computer Engineering, University of Tennessee, Knoxville. His research work has primarily focused on color image processing and 3-D computer vision, including stereo vision and laser range finding techniques. He

is a coauthor of two textbooks on 3-D image processing.

Dr. Koschan is a member of the Society for Imaging Science and Technology.



**Mongi Abidi** (S'83–M'85) received the Principal Engineer Diploma in electrical engineering from the National Engineering School of Tunis, Tunis, Tunisia, in 1981 and the M.S. and Ph.D. degrees in electrical engineering from the University of Tennessee, Knoxville, in 1985 and 1987, respectively.

He is currently a Professor and the Associate Department Head with the Department of Electrical and Computer Engineering, University of Tennessee, directing activities in the Imaging, Robotics, and Intelligent Systems Laboratory. His research work is

focused on 3-D imaging, in particular scene building, scene description, and data visualization.